Journal of Experimental Nanoscience
Publication details, including instructions for authors and subscription information:
http://www.informaworld.com/smpp/title~content=t716100757

Crystallite phase-controlled preparation, characterisation and photocatalytic properties of titanium dioxide nanoparticles

A. R. Khataee[a]; H. Aleboyeh[b]; A. Aleboyeh[b]
[a] Department of Applied Chemistry, Faculty of Chemistry, University of Tabriz, Tabriz, Iran [b] Laboratoire LPI, Groupe de Génie des Procédés de Traitement des Effluents, Ecole Nationale Supérieure de chimie de Mulhouse, Université de Haute Alsace, 68093 Mulhouse, France

To cite this Article Khataee, A. R. , Aleboyeh, H. and Aleboyeh, A.(2009) 'Crystallite phase-controlled preparation, characterisation and photocatalytic properties of titanium dioxide nanoparticles', Journal of Experimental Nanoscience, 4: 2, 121 — 137
To link to this Article: DOI: 10.1080/17458080902929945
URL: http://dx.doi.org/10.1080/17458080902929945

Journal of Experimental Nanoscience
Vol. 4, No. 2, June 2009, 121–137

Taylor & Francis
Taylor & Francis Group

Crystallite phase-controlled preparation, characterisation and photocatalytic properties of titanium dioxide nanoparticles

A.R. Khataee[a]*, H. Aleboyeh[b] and A. Aleboyeh[b]

[a]*Department of Applied Chemistry, Faculty of Chemistry, University of Tabriz, Tabriz, Iran;* [b]*Laboratoire LPI, Groupe de Génie des Procédés de Traitement des Effluents, Ecole Nationale Supérieure de chimie de Mulhouse, Université de Haute Alsace, 3, rue Alfred Werner, 68093 Mulhouse, France*

(*Received 12 February 2009; final version received 26 March 2009*)

A solution-based processing method has been used to synthesise nanostructured titanium dioxide (TiO_2) with different crystalline forms ratio (anatase, rutile and their mixtures) by controlling the hydrolysis of titanium tetrachloride in aqueous solution. The contents of anatase and rutile phases in the synthesised TiO_2 powders have been successfully controlled by simply changing the proportion of SO_4^{2-} in the aqueous phase. The prepared materials were characterised by X-ray diffraction, transmission electron microscopy, scanning electron microscope and Brunauer–Emmett–Teller techniques. The experimental results showed that the average size of the synthesised particles was in the range of 6–11 nm. The photocatalytic performance of the synthesised TiO_2 nanoparticles was evaluated by removal of the dye, C. I. Acid Blue 9 (AB9), under UV light illumination (30 W). According to the results, rutile appeared to be a poor photocatalyst while the mixed-phase TiO_2 (rutile–anatase) demonstrated the highest photoactivity. The efficiency parameters such as apparent quantum yield and electrical energy per order were estimated and compared for different crystalline forms of TiO_2. It was found that the photocatalysis process with synthesised mixed-phase TiO_2 nanoparticles, containing 70% anatase, had lower electrical energy consumption and higher quantum yield compared with others.

Keywords: nanoparticles; nano-TiO_2; photocatalyst; nanocatalyst; advanced oxidation processes

1. Introduction

Titanium dioxide (TiO_2) has attracted significant attention from researchers because of the many interesting physical and chemical properties that make it suitable for a variety of applications. For instance, TiO_2 has high corrosion resistance and chemical stability and an excellent optical transparency in the visible and near infrared regions, as well as a high refractive index that makes it useful for anti-reflection coatings in optical devices [1]. It has been used mostly as a pigment in paints, sunscreens, ointments and toothpaste since its commercial production in the early twentieth century. TiO_2 pigments are inorganic

*Corresponding author. Email: a_khataee@tabrizu.ac.ir

ISSN 1745–8080 print/ISSN 1745–8099 online

DOI: 10.1080/17458080902929945
http://www.informaworld.com

chemical products used for imparting whiteness, brightness and opacity to a diverse range of applications and end-use markets, including coatings, plastics, paper and other industrial and consumer products [2,3]. TiO_2 is obtained from a variety of ores that contain ilmenite, rutile, anatase and leucoxene, which are mined from deposits located throughout the world. Crystals of TiO_2 can exist in one of the three crystalline forms: rutile, anatase and brookite. Only anatase and rutile forms have good pigmentary properties, and rutile is more thermally stable than anatase. The crystallographic properties of rutile and anatase have been reported in Table 1 [4]. Most TiO_2 pigments have been produced from titanium mineral concentrates by the so-called chloride or sulphate process, either as the rutile or the anatase form.

Since the discovery of photocatalytic splitting of water on TiO_2 electrodes [5], efforts have been devoted to the development of efficient water and air purification technologies, based on TiO_2 photocatalysis. Such treatments typically oxidise toxic organic compounds to non-toxic inorganic compounds, such as carbon dioxide, water, ammonium or nitrates, and chloride ions [6].

In the framework of the rapid development of nanoscience and nanotechnology, the domain of nanostructured materials, such as nanostructured TiO_2, is necessitating more research, both of an academic and of an industrial nature. Synthesis methods are a major prerequisite for achievement in this rapidly evolving field. The essential first step in the use of nanomaterials in various technologies is their production [7,8].

There are many methods of producing nanostructured TiO_2, such as the hydrothermal method [9,10], sol–gel technique [11,12], chemical vapour deposition (CVD) [13–15], physical vapour deposition [16,17], solvothermal method [18,19], electrochemical approaches (e.g. anodising of Ti) [20–22], solution combustion method [23–25], microemulsion [26,27], micelle and inverse micelle methods [28,29], ball milling [30], a flame by vapour phase [31], sonochemical reactions [32] and plasma evaporation [33,34]. It should be noted that as precursors of nanocrystalline oxide powders, however, inorganic compounds are more economical than alkoxides. Since the phases and morphologies of TiO_2 are critical parameters in determining their suitability for particular applications, it is still necessary to explore new methods for synthesising nanostructured TiO_2, and especially to explore the methods fit for selectively preparing various TiO_2 phases (anatase, rutile and their mixtures).

Therefore, in this work, the solution-based processing method has been used to synthesise various crystalline phases of nanostructured TiO_2 including anatase, rutile and their mixtures, by controlling the hydrolysis of $TiCl_4$ in aqueous solution. The photocatalytic activity of the synthesised nanostructured TiO_2 samples has been tested in decolorisation of the dye solution containing C. I. Acid Blue 9.

Table 1. Crystallographic properties of rutile and anatase [4].

				Cell parameters (nm)		
Crystal structure	Density ($kg\,m^{-3}$)	System	Space group	A	*b*	C
Rutile	4240	Tetragonal	$D_{4h}^{14} - P4_2/mnm$	0.4584		0.2953
Anatase	3830	Tetragonal	$D_{4\alpha}^{19} - I4_1/amd$	0.3758		0.9514

C. I. Acid Blue 9, which belongs to the acidic dyes group, is soluble in cold water and methanol. It can be found in textile (as a dye for wool and silk), foodstuff and pharmaceutical wastewaters. In addition, C. I. Acid Blue 9 is the principal active ingredient in Aquashade, which can be used as an aquatic algaecide/herbicide, in natural or manmade ponds, lakes, fountains, fish farms and fish hatcheries, and may be applied by both professional applicators and homeowners. It is hazardous in case of ingestion, skin contact (irritant), eye contact (irritant), and inhalation [35,36].

2. Experimental details

2.1. *Reagents*

All inorganic compounds were obtained from Merck, Germany. C. I. Acid Blue 9 was obtained from Shimi Keshavarz Company, Iran. Its structure and characterisation are given in Table 2.

2.2. *Preparation of TiO_2 nanoparticles*

The nanocrystalline TiO_2 reported in this study was prepared by $TiCl_4$ hydrolysis. Titanium tetrachloride (98% $TiCl_4$) was used as a main starting material without any further purification. The appreciated amount of $TiCl_4$ was dissolved in distilled water in an ice-water bath (Figure 1). The concentration of titanium was adjusted to 3 M. This aqueous solution was then mixed with $(NH_4)_2SO_4$ solution for preparation of anatase in a temperature-controlled bath. The mixture was stirred at high speed while the amount of

Table 2. Structure and characteristics of C. I. Acid Blue 9.

Other names	Brilliant Blue FCF, Erioglaucine, C.I. Food Blue 2, Brilliant Blue FCF, FD&C Blue no. 1
Colour index (C. I.) no.	42090
Molecular formula	$C_{37}H_{34}N_2Na_2O_9S_3$
Molecular mass	792.86 ($g\,mol^{-1}$)
Absorption maximum (λ_{max})	625 (nm)
CAS No.	3844-45-9
Aqueous solubility	200 $kg\,m^{-3}$
Chemical class	Triphenylmethan dye
Chemical structure	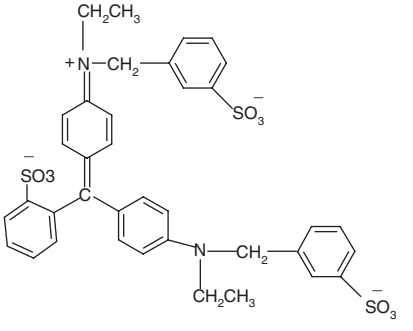

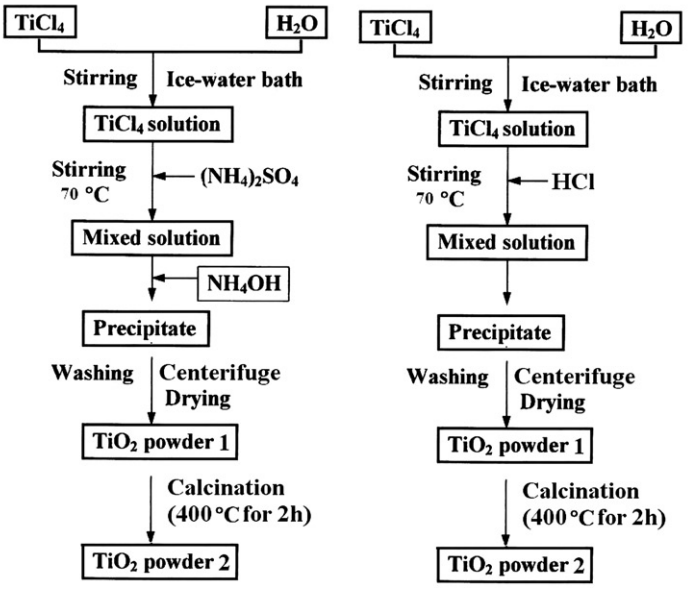

Figure 1. Flow chart of the steps involved in the preparation of TiO_2 nanoparticles of anatase (left) and rutile (right).

$TiCl_4$ solution necessary for the desired [H_2O]: [Ti] molar ratio was added dropwise. Having maintained it at the hydrolysis temperature (70°C) for 1 h, the mixed solution was treated with 2.5 M dilute NH_4OH until the pH value was 7. For preparation of rutile crystalline, the $TiCl_4$ solution was diluted with 0.5 M HCl solution (70°C) and was not treated with NH_4OH solution. Then, the mixed solution was placed into a constant temperature (70°C) bath for 5 h. Subsequently, the precipitated titanium oxide (TiO_2–nH_2O) was separated from the solution by using centrifugation and repeatedly washed with distilled water to make TiO_2–nH_2O that was free of chloride ions. The hydrous titanium oxide was dried at 110°C under vacuum and ground to fine powder (TiO_2 powder 1), then was calcined at 400°C for 2 h (Figure 1). For preparation of a mixture of anatase and rutile phase TiO_2 powder, a small amount of $(NH_4)_2SO_4$ was added and the concentration of $TiCl_4$ was adjusted to 0.5 M with distilled water. The rest of the preparation steps are just like the preparation method of anatase in a temperature-controlled bath.

2.3. *Characterisation of the nanostructured TiO_2*

To determine the crystal phase composition and average crystalline size of synthesised nanostructured TiO_2 samples, X-ray diffraction (XRD) measurements were carried out at room temperature by using Siemens XRD D5000, with Cu Kα radiation. The accelerating voltage of 40 kV and emission current of 30 mA was used. The average crystalline size of the samples was calculated according to Debye–Scherrer formula [37]:

$$D = \frac{0.9\lambda}{\beta \cos\theta} \quad (1)$$

where D is the average crystallite size (Å), λ is the wavelength of the X-ray radiation (Cu K$\alpha = 1.54178$ Å), β is the full width at half maximum (fwhm) intensity of the peak and θ is the diffraction angle. The weight fraction of the anatase and rutile present in the samples was estimated based on the most signal of each phase (anatase and rutile) according to the equation described by Spurr and Myers [38]:

$$x_A = \frac{100}{1 + [(I_R)/(0.8I_A)]} \tag{2}$$

where x_A is the weight fraction of the anatase phase present in the powder sample, while I_A and I_R are the relative reflection intensities of anatase and rutile, respectively.

The samples used for transmission electron microscopy (TEM) observations were prepared by dispersing the powders in distilled water followed by ultrasonic vibration (Sonoplus Ultrasonic Homogeniser HD 2200, Germany) for 15 min, then placing a drop of the dispersion onto a copper grid coated with a layer of amorphous carbon. A LEO 906 (60 kV) TEM was used to study the morphology. The surface morphology of the catalysts was observed by scanning electron microscope (SEM). The samples for SEM imaging were coated with a thin layer of gold film to avoid charging. A LEO 440i SEM was used to study the morphology.

Nitrogen sorption analyses were obtained with a Micromeritics Tristar sorptometer using standard continuous procedures at 77.15 K on calcined samples that had been degassed at 363 K for 1 h and then at 403 K under high vacuum for at least 10 h. Surface area was calculated according to the Brunauer–Emmett–Teller (BET) model [39] over a relative pressure range of 0.05–0.30. Pore diameter distribution was calculated according to the Barret–Joyner–Halenda (BJH) method [39], modified by the Halsey thickness curve correction [40] on the desorption branch.

2.4. *Photocatalytic experiments*

The photocatalytic test-reaction chosen to characterise the different synthesised nanostructured TiO_2 samples was the decolorisation of the dye solution containing C. I. Acid Blue 9, selected as a model organic pollutant. In the UV/TiO_2 process, irradiation was carried out with a 30 W (UV-C) mercury lamp (Philips, Holland), which was put above a batch photocatalytic reactor of 500 mL in volume. On the surface of the solution, the light intensity was measured by Cassy Lab, Germany. The desired concentration of C. I. Acid Blue 9 (20 mg L^{-1}) and TiO_2 were fed into the pyrex reactor. The TiO_2 suspension was sonicated for 15 min, before illumination, to disperse TiO_2 uniformly in the solution by sonoplus ultrasonic homogeniser HD 2200, Germany. The value of incident photon flux by reactor volume unit at 254 nm was 2.33×10^{-6} Einstein L^{-1} s^{-1}, which was calculated on the base of ferrioxalate actinometry measurement [41]. The pH of the solution was adjusted using dilute solutions of sulphuric acid and aqueous sodium hydroxide when necessary and measured by pH meter (Metrohm, Switzerland). The UV lamp was switched on to initiate the reaction. During the irradiation, agitation was maintained to keep the solution homogenous and to increase mass transfer coefficient and, as a result, the overall dye decomposition rate. At specific time intervals, the concentration of the dye in each sample was determined using a Lightwave S2000 (England) UV/Vis spectrophotometer at $\lambda_{max} = 625$ nm. A linear correlation was established between the dye

concentration and the absorbance at $\lambda_{max} = 625\,nm$, in the range of 0–35 mg L^{-1} with a coefficient of correlation $r^2 = 0.9993$. The equation used to calculate the photocatalytic removal efficiency (X) in the treatment experiments was:

$$X = \left(\frac{C_0 - C}{C_0}\right) \tag{3}$$

where C_0 was the initial concentration of the dye (mg L^{-1}) and C was the concentration of the dye (mg L^{-1}) at time t.

3. Results and discussion

3.1. *Preparation mechanism of different crystallite phases of TiO_2*

The mechanism of forming different crystallite phases of nanostructured TiO_2 has been showed in Figure 2. From metal halide to the formation of metal oxide, there are two processes: hydrolysis and polycondensation [42]. When the titanic halide reacts with water, the titanium ion first increases its coordination by using its vacant d orbitals to accept oxygen electron pairs from nucleophilic ligands (such as −OH groups) [43]. Consequently, the titanium ion forms an octahedral structure of $(Ti(O)_m(OH)_n(H_2O)_{6-m-n})^{(2m+n-4)-}$. Because the reaction is performed under an acidic medium, only −OH and $-OH_2$ groups will be present, and the octahedral structure of the titanium ion becomes $(Ti(OH)_m(H_2O)_{6-m})^{(m-4)-}$ [44]. Then, the structures dehydrate each other and poly-condensed into the final precipitate.

Crystals of TiO_2 can exist in one of the three crystalline forms: rutile, anatase or brookite (Table 1). In their structures, the basic building block consists of a titanium atom surrounded by six oxygen atoms in a more or less distorted octahedral configuration. In all three TiO_2 structures, the stacking of the octahedra results in three-fold coordinated oxygen atoms. The fundamental structural units in these three TiO_2 crystals forming from TiO_6 octahedron units and having different modes of arrangement and links as presented in Figure 2. In the rutile form, TiO_6 octahedra link by sharing an edge along the c-axis to form chains. These chains are then interlinked by sharing corner oxygen atoms to form a three-dimensional framework, whereas in anatase, the three-dimensional framework is formed only by edge-shared bonding among TiO_6 octahedrons. It means that octahedra in anatase share four edges and are arranged in zigzag chains along [44–48].

As can be seen in Figure 2, for forming anatase and rutile nuclei, the placement of the third octahedron is very important and determines whether a rutile or an anatase nucleus is formed. However, the presence of SO_4^{2-} would influence the orientation of the third octahedron. When SO_4^{2-} ions exist in the acid reaction media, these ions would interact with octahedral hydroxyls by static electricity. Because of the steric effect of SO_4^{2-}, the octahedron with SO_4^{2-} and another octahedron would polycondense along the converse direction in order to decrease the repulsion, and the orientation of the third octahedron is more conducive to the formation of an anatase nucleus. The more the SO_4^{2-}, the more anatase nuclei can be formed. TiO_2 clusters grow further on the nucleus and then form the anatase phase. It has been reported that the presence of SO_4^{2-} accelerated the growth of TiO_2 clusters to anatase [47,48]. As a result, different rutile/anatase mixtures can be prepared by changing the proportion of SO_4^{2-} in the aqueous phase. On the other hand,

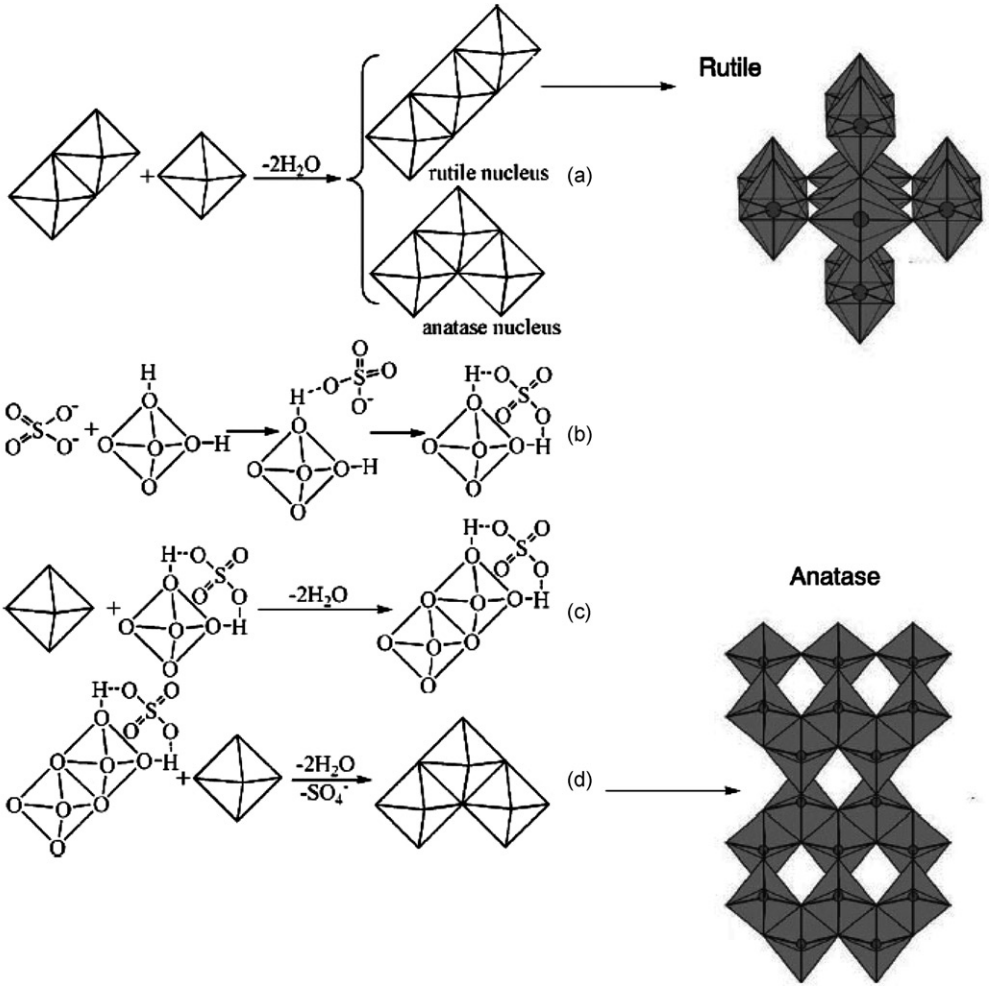

Figure 2. Proposed mechanism for preparation of TiO_2 with rutile or anatase phases: (a) the orientation of the third octahedron determines whether a rutile or an anatase nucleus is formed; (b) interaction between SO_4^{2-} and TiO_6^{2-} octahedral hydroxyls; (c) two TiO_6^{2-} octahedra share edge in the presence of SO_4^{2-}; (d) formation of anatase in the presence of SO_4^{2-}.

there is a weak steric effect for Cl^- because of its small radius. Meanwhile, the addition of Cl^- generally favours the formation of rutile crystallites [47–49].

As was mentioned, TiO_2 is known to possess three crystalline structures, which include rutile, anatase and brookite. In coming up with these crystal structures and to estimate the crystal grain size of anatase, rutile and brookite, the XRD experimental method is used. The XRD patterns of the synthesised anatase, rutile and their mixture have been reported in Figure 3. It can be observed from Figure 3 that anatase peaks in XRD are at $2\theta = 25.3^\circ$, 37.8°, and 48.1°, while the rutile peaks are at $2\theta = 27.5^\circ$, 36.2°, and 54.4°, where θ is the XRD angle. This result confirmed that the addition of sulphate was quite effective in promoting the formation of the anatase phase as the pH value rose as a result of the

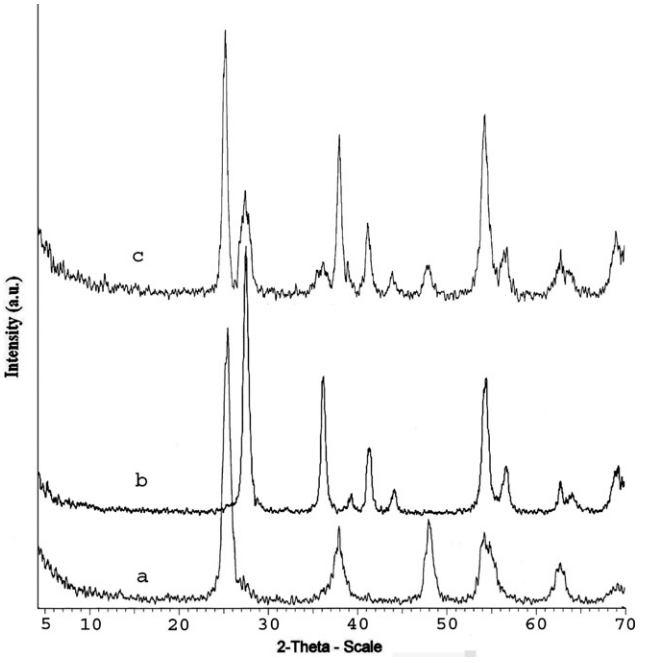

Figure 3. X-ray diffraction (XRD) patterns of synthesised TiO_2 samples: (a) anatase, (b) rutile (c) rutile–anatase.

Table 3. Physicochemical characteristics of the synthesised TiO_2 nanoparticles.

Crystalline phase of synthesised TiO_2 sample	Anatase	Rutile	Anatase–Rutile
Anatase content (wt%) by XRD	100	0	70
Average crystallite size (nm)	8	11	6–10
BET surface area ($m^2 g^{-1}$)	119.96	28.31	75.29
Total pore volume ($cm^3 g^{-1}$)	0.3197	0.0747	0.2069
Pore size (nm)	9.59	10.11	12.92

neutralisation of NH_4OH. The characteristics of the synthesised nanostructured TiO_2 have been reported in Table 3. The TEM images of the synthesised TiO_2 have been shown in Figure 4. These show the size distribution of TiO_2 particles. The average diameter of the particles measured from the TEM images is in good agreement with XRD results.

The prepared TiO_2 powders, either in the presence of SO_4^{2-} ions or not, dried at room temperature under vacuum, were dominantly amorphous (Figure 5). The morphology of the amorphous TiO_2 powder observed by SEM is shown in Figure 5.

3.2. *Photocatalytic activity of the synthesised TiO_2 nanoparticles*

The photocatalytic decolorisation of the solution containing C.I. Acid Blue 9 under UV illumination was used to evaluate the photoactivity of the synthesised TiO_2 nanoparticles.

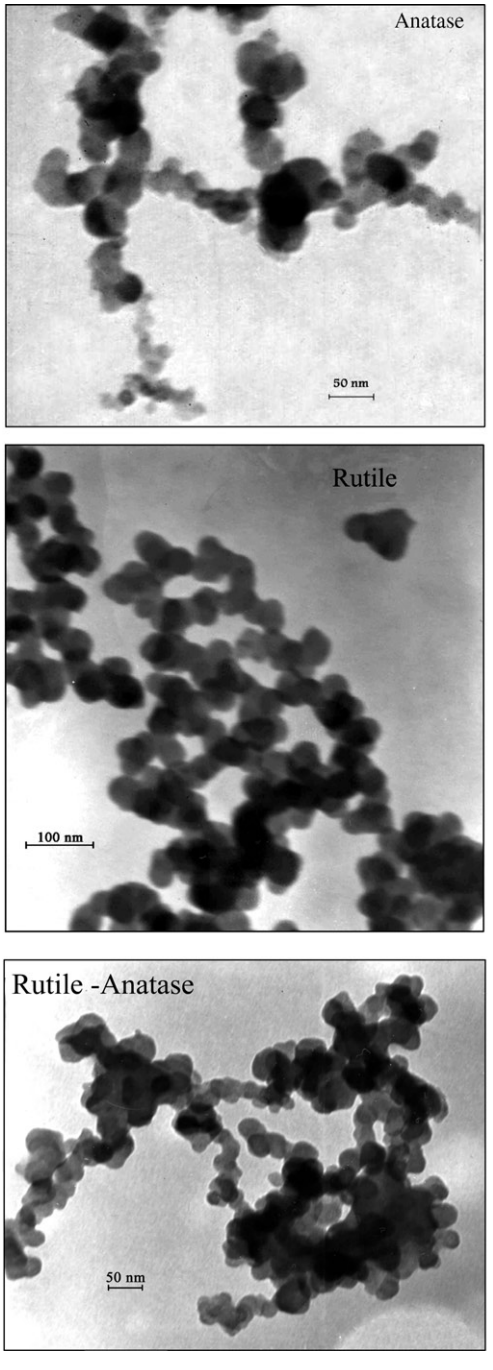

Figure 4. TEM images of the synthesised TiO_2 samples calcined at 400°C for 2 h.

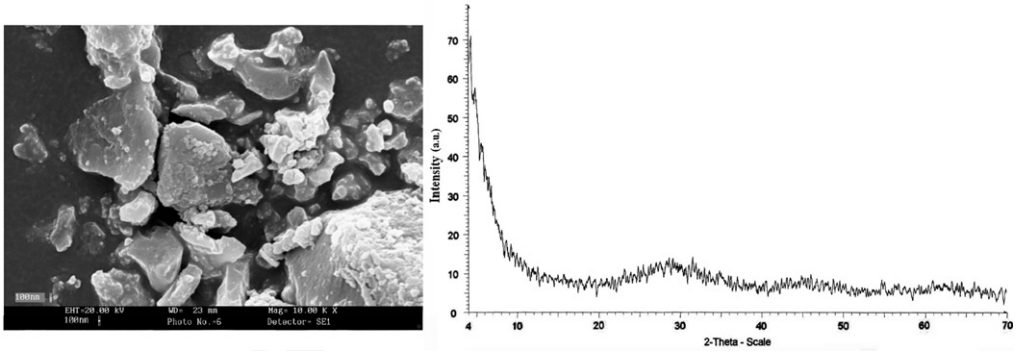

Figure 5. SEM image (left) and XRD pattern (right) of the amorphous TiO_2 powder dried at room temperature under vacuum.

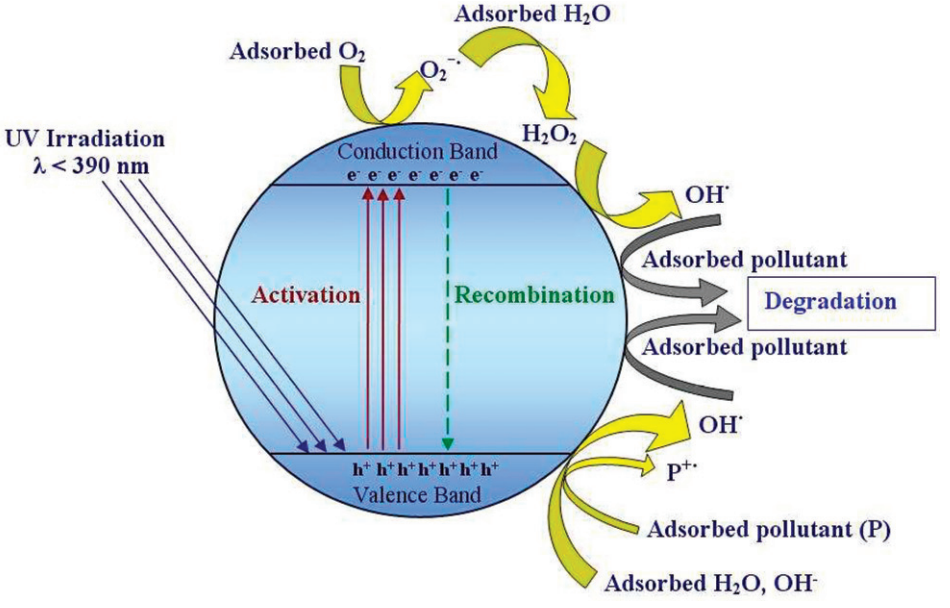

Figure 6. General mechanism of the photocatalysis on TiO_2 nanoparticle.

We found that TiO_2 and UV light had a negligible effect when they were used on their own. The reason for this observation is due to the fact that when TiO_2 is illuminated with light of energy greater than its optical band gap ($\lambda < 390$ nm), an electron is transferred to the conduction band, leaving a hole in the valance band. This is called production of an electron-hole (e^-/h^+) pair. At the solid liquid interface, electron transfer can occur both from the conduction band to an electron acceptor (O_2, H^+, etc.) in the solution and from a donor (OH^-, H_2O, organic pollutants (P), etc.) in the solution to the valence band hole. Moreover, the hydroxyl radicals formed are strong oxidants and attack organic pollutants present at or near the surface of TiO_2. This causes photodegradation of pollutants [50–52]. The mechanism is assumed up in Figure 6.

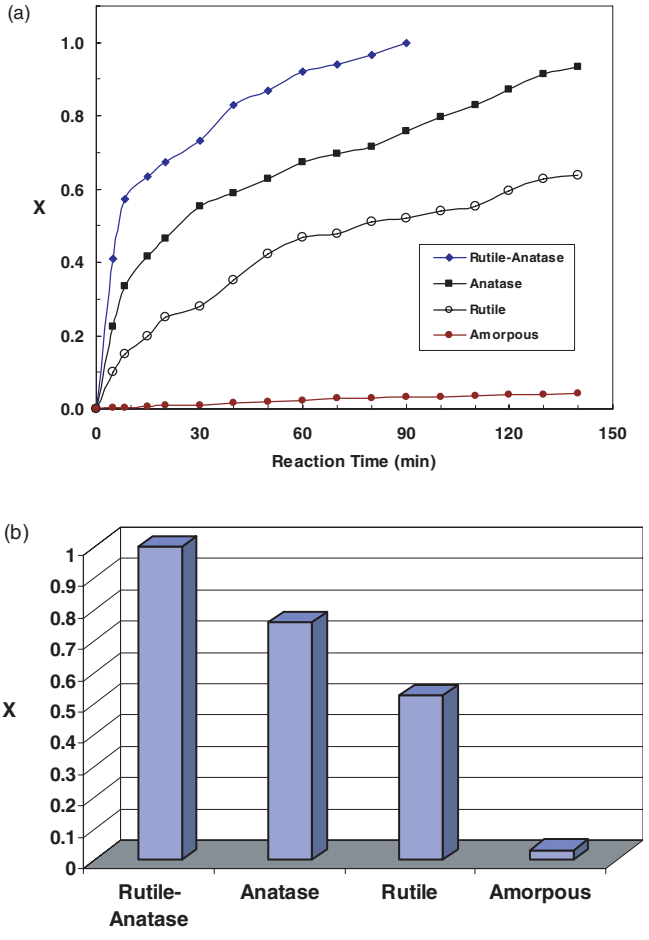

Figure 7. Comparison of the photocatalytic activity of different synthesised TiO_2 nanoparticles. $[TiO_2]_0 = 150\,mg\,L^{-1}$, $[AB9]_0 = 20\,mg\,L^{-1}$, pH = 6.2, $V = 50\,mL$, $I = 11.2\,W\,m^{-2}$: (a) during different irradiation times, (b) at the irradiation time of 90 min.

The characteristic absorbance at 625 nm of AB9 solution was monitored during the reaction process. Comparison of the photocatalytic activity of different synthesised TiO_2 nanoparticles has been shown in Figure 7. It is clear that the photocatalytic activity of amorphous TiO_2 is negligible. As can be seen from Figure 7, rutile appeared to be a poor photocatalyst while the mixed-phase TiO_2 (rutile–anatase) demonstrated the highest photoactivity. In a recent study by Gray et al. [53], mixed-phase TiO_2 nanocomposites were synthesised using a hydrothermal method for photooxidation and photoreduction applications. These authors found that the anatase–rutile nanocomposite exhibited the highest photoactivity among the catalysts tested. They also claim that a synergic effect exists between the anatase and rutile particles, in which spatial charge separation hinders charge recombination [53]. In addition, it has long been empirically observed that mixed-phase TiO_2, i.e. TiO_2 containing both anatase and rutile, tends to exhibit higher

photocatalytic activities than pure-phase TiO_2. When Bacsa and Kiwi [54] prepared TiO_2 samples with different ratios of anatase : rutile, the highest photoactivity was obtained with a 70 : 30 ratio, which is similar to that of Degussa P25. In our study, the anatase : rutile ratio of the mixed-phase TiO_2 was 70 : 30 (Table 3).

A possible reason for the improved performance of such mixed-phase TiO_2 samples is that rutile acts as a sink for the electrons generated in anatase, serving to physically separate the electron-hole and thereby depress rates of recombination [55] (Figure 8(a)). This model is consistent with the fact that the band edges of rutile lie within those of anatase; i.e. the potential of the conduction band edge of anatase is more negative than that of rutile. However, it has been recently shown that just the opposite occurs: rutile undergoes band gap activation, and electrons are shuttled from rutile to anatase sites, which must be of lower energy (Figure 8(b)). This implies that one or more trap sites exist on anatase at potentials more positive than the conduction band edge of either anatase or rutile. This was recently confirmed by a photoacoustic spectroscopy study of anatase, which found trap sites on anatase at an average of 0.8 eV below the conduction band edge [55,56].

It can be concluded that the size and morphology of rutile and anatase nanocrystals are critical to the separation and enhanced activity of mixed-phase TiO_2. As was illustrated in Figure 8(b), an emerging model of mixed-phase TiO_2 particles describes an atypically small rutile core surrounded by anatase crystallites. Catalytic 'hot spots' are believed to exist at the intersection of the two phases, where distorted geometry gives rise to unique surface chemistry.

The photocatalytic activity of TiO_2 materials can be influenced by many factors, including crystal structure, particle size, surface area, porosity, density of surface hydroxyl groups, surface acidity, number and nature of trap sites, and adsorption–desorption characteristics [35,53]. For a catalyst, a key requirement to demonstrate high activity is to have the small primary particle size and high surface area. As can be seen in Table 3, the

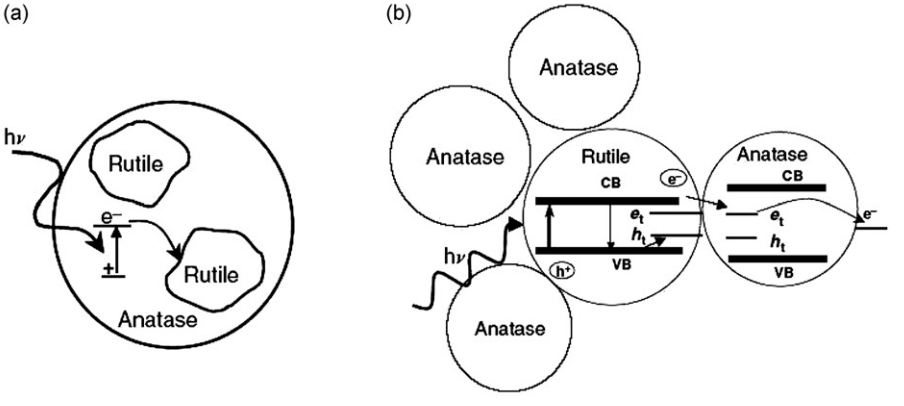

Figure 8. Models of mixed-phase TiO_2: (a) rutile islands surround anatase particles, and rutile is an electron sink; (b) a small rutile core surrounded by anatase crystallites, where electrons are shuttled from rutile to anatase.

primary particle size of the synthesised mixed-phase TiO_2 (6–10 nm) is smaller than that others.

Figure 9 shows a typical time-dependent UV-Vis spectrum of AB9 solution during photocatalysis. The spectrum of AB9 in the visible region exhibits a main band with a maximum at 625 nm. As is clear from this figure, the absorption peaks diminished and finally disappeared under reaction, which indicated that the AB9 had been destructed. No new absorption bands appear in either the visible or ultraviolet regions. Complete decolorisation of the dye solution was observed after 90 min in the optimised conditions. Since photocatalysis of aqueous organic pollutant is an electric-energy-intensive process, and electric energy can represent a major fraction of the operating costs, simple figures-of-merit based on electric energy consumption can be very useful and informative. The photochemistry commission of the International Union of Pure and Applied Chemistry (IUPAC) proposed a figure-of-merit (or more appropriately, an Efficiency Index, as it compares electrical efficiency of different AOPs) for UV-based AOPs [57]. Electrical energy per order (E_{EO}) compares electrical efficiency of different UV-based AOPs and is a measure of the electrical efficiency of an AOP system. It is defined (for low concentration of pollutants) as the electrical energy in kilowatt hours (kWh) required bringing about the degradation of a contaminant by one order of magnitude in $1m^3$ (1000 L) of contaminated water. Generally, the higher the energy efficiency of a process, the lower the E_{EO}. The values of E_{EO} can be calculated using the following Equation [57,58]:

$$E_{EO} = \frac{\text{Lamp power (kW)} \times \text{(min)} \times 1000}{\text{Treated volume (1)} \times 60 \times \log(C_0/C)} = \frac{38.4 \times P}{V \times k_{app}} \quad \text{Batch operation} \qquad (4)$$

The electric dose (kWh m^{-3} $order^{-1}$) required to oxidise C. I. Acid Blue 9 (20 mg L^{-1}) in the presence of synthesised TiO_2 nanoparticles has been reported in Table 4. It is clear that a photocatalytic process with synthesised mixed-phase TiO_2 nanoparticles offered the best energy efficiency. Finally, it is useful to relate the E_{EO} values found in this study to the treatment costs. For instance, if the cost of the electricity in Iran and France is \$0.0065 and

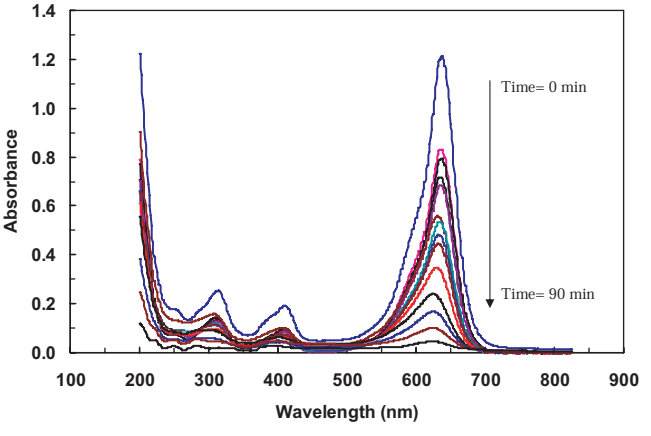

Figure 9. UV-Vis spectrum of AB9 (20 mg L^{-1}) during photocatalysis in the presence of the synthesised mixed-phase TiO_2 nanoparticles. $[TiO_2]_0 = 150$ mg L^{-1}, pH = 6.2, $I = 11.2$ W m^{-2}.

Table 4. Rate constants, half-lives, electrical energy per order and apparent quantum yield for photocatalytic decolorisation of AB9 in the presence of the synthesised TiO_2 nanoparticles. $[AB9]_0 = 20\,mg\,L^{-1}$, $[TiO_2]_0 = 150\,mg\,L^{-1}$, pH = 6.2.

Crystalline phase of synthesised TiO_2 sample	k (min^{-1})	R^2	$t_{1/2}$ (min)	E_{EO} ($kWh\,m^{-3}$ $order^{-1}$)	$\varphi_{app} \times 10^{-3}$
Rutile–Anatase	0.0374	0.98	18.53	616	6.75
Anatase	0.0159	0.96	43.59	1449	2.87
Rutile	0.0067	0.97	103.45	3439	1.21

\$0.092 per kWh, the contribution to treatment cost of $20\,mg\,L^{-1}$ AB9 solution, in the presence of the mixed-phase TiO_2, from electrical energy will be \$ 4.0 and \$ 56.7 per m^3, respectively. In addition there will be smaller cost factors for the photocatalyst used and for UV lamp replacement.

The efficiency of the heterogeneous photocatalytic process can be quantified in term of quantum yield, which may be defined as the rate at which reactant molecules disappear or product molecules form, divided by the number of photons absorbed per unit time. In our study, the apparent quantum yield of photocatalysis process has been calculated by Equations (5) and (6) [59,60]:

$$\text{Apparent quantum yield } (\varphi_{app}) = \frac{\text{Rate of disappearance of reactant molecules}}{\text{Rate of incident photons inside reactor}} \quad (5)$$

$$\varphi_{app} = \frac{k \times C_0}{I_0} \quad (6)$$

where k (s^{-1}) is the apparent first-order rate constant, C_0 ($mol\,L^{-1}$) is the initial dye concentration and I_0 (Einstein $L^{-1}\,s^{-1}$) is the total intensity of incident photons entering the reactor. The apparent quantum yield for oxidation of C. I. Acid Blue 9 ($20\,mg\,L^{-1}$) in the presence of synthesised TiO_2 nanoparticles has been reported in Table 4. As seen in Table 4, the photocatalytic process with synthesised mixed-phase TiO_2 nanoparticles has lower electrical energy consumption and higher quantum yield compared with others.

4. Conclusions

TiO_2 nanoparticles in anatase, rutile and their mixture phases have been synthesised from aqueous solution of $TiCl_4$. The addition of a small amount of $(NH_4)_2SO_4$ promoted occurrence of anatase phase and inhibited the anatase–rutile transformation such that the powder was completely anatase after calcining at 400°C for 2h. The anatase–rutile mixture (70 : 30) was prepared by controlling the proportion of SO_4^{2-} in the aqueous phase. The synthesised TiO_2 samples have narrow size distribution and their average particle size was 6–11 nm. The mixed-phase TiO_2 nanoparticles have reasonable photocatalytic efficiencies, and nearly complete of C. I. Acid Blue 9 was removed in 90 min. The values of electric energy per order and apparent quantum yield calculated in the presence of different synthesised TiO_2 samples, demonstrated that the most efficient process was that using mixed-phase TiO_2 nanoparticles containing 70% anatase.

Acknowledgements

The authors thank the University of Tabriz, Iran for financial and other supports.

References

[1] C.X. Shan, X. Hou, and K. Choy, *Corrosion resistance of TiO_2 films grown on stainless steel by atomic layer deposition*, Surf. Coat. Tech. 202 (2008), pp. 2399–2402.
[2] P. Boisvert, J. Persello, A. Foissy, J. Castaing, and B. Cabane, *Effect of surface charge on the adsorption mode of sodium poly(acrylate) on alumina-coated TiO_2 used as coating pigment*, Colloid Surf. A 168 (2000), pp. 287–296.
[3] R. Zallen and M.P. Moret, *The optical absorption edge of brookite TiO_2*, Solid State Commun. 137 (2006), pp. 154–157.
[4] M. Zheng, M. Gu, Y. Jin, and G. Jin, *Preparation, structure and properties of TiO_2–PVP hybrid films*, Mat. Sci. Eng. B: Solid 77 (2000), pp. 55–59.
[5] A. Fujishima and K. Honda, *Electrochemical photolysis of water at a semiconductor electrode*, Nature 238 (1972), pp. 37–38.
[6] N. Daneshvar, D. Salari, and A.R. Khataee, *Photocatalytic degradation of azo dye acid red 14 in water: investigation of the effect of operational parameters*, J. Photochem. Photobiol. A 157 (2003), pp. 111–116.
[7] T. Yates Jr and L. Thompson, *Surface science studies of the photoactivation of TiO_2— new photochemical processes*, Chem. Rev. 106 (2006), pp. 4428–4453.
[8] X. Chen and S.S. Mao, *Titanium dioxide nanomaterials: synthesis, properties, modifications, and applications*, Chem. Rev. 107 (2007), pp. 2891–2959.
[9] K. Mori, K. Maki, S. Kawasaki, S. Yuan, and H. Yamashita, *Hydrothermal synthesis of TiO_2 photocatalysts in the presence of NH4F and their application for degradation of organic compounds*, Chem. Eng. Sci. 63 (2008), pp. 5066–5070.
[10] G. Wang, *Hydrothermal synthesis and photocatalytic activity of nanocrystalline TiO_2 powders in ethanol–water mixed solutions*, J. Molecular Catal. 274 (2007), pp. 185–191.
[11] L. Kao, T. Hsu, and H. Lu, *Sol-gel synthesis and morphological control of nanocrystalline TiO_2 via urea treatment*, J. Colloid Interf. Sci. A 316 (2007), pp. 160–167.
[12] Q. Xiao, Z. Si, Z. Yu, and G. Qiu, *Sol-gel auto-combustion synthesis of samarium-doped TiO_2 nanoparticles and their photocatalytic activity under visible light irradiation*, Mat. Sci. Eng. B: Solid 137 (2007), pp. 189–194.
[13] X. Zhang, M. Zhou, and L. Lei, *Preparation of anatase TiO_2 supported on alumina by different metal organic chemical vapor deposition methods*, Appl. Catal. A 282 (2005), pp. 285–293.
[14] S. Jung, S. Kim, N. Imaishi, and Y. Cho, *Effect of TiO_2 thin film thickness and specific surface area by low-pressure metal–organic chemical vapor deposition on photocatalytic activities*, Appl. Catal. B 55 (2005), pp. 253–257.
[15] Y. Su, X. Zhang, S. Han, X. Chen, and L. Lei, *F-B-codoping of anodized TiO_2 nanotubes using chemical vapor deposition*, Electrochem. Commun. 9 (2007), pp. 2291–2298.
[16] C. Giolli, F. Borgioli, A. Credi, A. Fabio, A. Fossati, M. Miranda, S. Parmeggiani, G. Rizzi, A. Scrivani, and S. Troglio, *Characterization of TiO_2 coatings prepared by a modified electric arc-physical vapour deposition system*, Surf. Coat. Tech. 202 (2007), pp. 13–22.
[17] S. Chiu, Z. Chen, K. Yang, Y. Hsu, and D. Gan, *Photocatalytic activity of doped TiO_2 coatings prepared by sputtering deposition*, J. Mater. Process. Tech. 192–193 (2007), pp. 60–67.
[18] M. Kang, *The superhydrophilicity of Al–TiO_2 nanometer sized material synthesized using a solvothermal method*, Mater. Lett. 59 (2005), pp. 3122–3127.
[19] R.K. Wahi, Y. Liu, C.J. Falkner, and L.V. Colvin, *Photocatalytic activity of doped TiO_2 coatings prepared by sputtering deposition*, J. Colloid Interf. Sci. 302 (2006), pp. 530–536.

[20] B.R. Sankapal, S.D. Sartale, M.C. Lux-Steiner, and A. Ennaoui, *Chemical and electrochemical synthesis of nanosized TiO_2 anatase for large-area photon conversion*, Compt. Rendus Chim. 9 (2006), pp. 702–707.
[21] E.H. Prakasam, K. Shankar, M. Paulose, K.O. Varghese, and C.A. Grimes, *A new benchmark for TiO_2 nanotube array growth by anodization*, J. Phys. Chem. C 111 (2007), pp. 7235–7241.
[22] N.R. Tacconi, C.R. Chenthamarakshan, G. Yogeeswaran, A. Watcharenwong, R.S. Zoysa, A.N. Basit, and K. Rajeshwar, *Nanoporous TiO_2 and WO_3 films by anodization of titanium and tungsten substrates: influence of process variables on morphology and photoelectrochemical response*, J. Phys. Chem. A 110 (2006), pp. 25347–25355.
[23] K. Nagaveni, G. Sivalingam, M.S. Hegde, and G. Madras, *Photocatalytic degradation of organic compounds over combustion-synthesized nano-TiO_2*, Environ. Sci. Technol. 38 (2004), pp. 1600–1604.
[24] G. Sivalingam, M.H. Priya, and G. Madras, *Kinetics of the photodegradation of substituted phenols by solution combustion synthesized TiO_2*, Appl. Catal. B 51 (2004), pp. 67–76.
[25] G. Sivalingam and G. Madras, *Photocatalytic degradation of poly(bisphenol-A-carbonate) in solution over combustion-synthesized TiO_2: mechanism and kinetics*, Appl. Catal. A 269 (2004), pp. 81–90.
[26] T. Mishra, *Anion supported TiO_2–ZrO_2 nanomaterial synthesized by reverse microemulsion technique as an efficient catalyst for solvent free nitration of halobenzene*, Catal. Commun. 9 (2008), pp. 21–26.
[27] M. Lee, G. Lee, C. Ju, and S. Hong, *Preparations of nanosized TiO_2 in reverse microemulsion and their photocatalytic activity*, Sol. Energ. Mat. Sol. C. 88 (2005), pp. 389–401.
[28] T. Ohno, R. Inaba, T. Fukahori, and M. Hamamoto, *Preparation of S-doped TiO_2 photocatalysts and their photocatalytic activities under visible light*, J. Molecular Catal. A 260 (2006), pp. 247–254.
[29] X. Sui, Y. Chu, S. Xing, M. Yu, and C. Liu, *Self-organization of spherical PANI/TiO_2 nanocomposites in reverse micelles*, Colloid. Surface. A 251 (2004), pp. 103–107.
[30] C. Shifu, C. Lei, G. Shen, and C. Gengyu, *The preparation of nitrogen-doped photocatalyst $TiO_{2-x}N_x$ by ball milling*, *Chem*. Phys. Lett. 413 (2005), pp. 404–409.
[31] B.K. Kim, G.G. Lee, M.H. Park, and N.J. Kim, *Characteristics of nanostructured TiO_2 powders synthesized by combustion flame-chemical vapor condensation process*, Nanostruct. Mater. 12 (1999), pp. 637–640.
[32] W. Guo, Z. Lin, X. Wang, and G. Song, *Sonochemical synthesis of nanocrystalline TiO_2 by hydrolysis of titanium alkoxides*, Microelectron. Eng. 66 (2003), pp. 95–101.
[33] T. Miyata, S. Tsukada, and T. Minami, *Preparation of anatase TiO_2 thin films by vacuum arc plasma evaporation*, Thin Solid Films 496 (2006), pp. 136–140.
[34] H. Huang and X. Yao, *Preparation and characterization of rutile TiO_2 thin films by mist plasma evaporation*, Surf. Coat. Tech. 191 (2005), pp. 54–58.
[35] N. Daneshvar, D. Salari, A. Niaei, and A.R. Khataee, *Photocatalytic degradation of the herbicide erioglaucine in the presence of nanosized titanium dioxide: comparison and modeling of reaction kinetics*, J. Environ. Sci. Health B 41 (2006), pp. 1273–1290.
[36] M. Flury and H. Flühler, *Tracer characteristics of brilliant blue FCF*, Soil Sci. Soc. Am. J. 59 (1995), pp. 22–27.
[37] A.L. Patterson, *The scherrer formula for x-ray particle size determination*, Phys. Rev. 56 (1939), pp. 978–982.
[38] R.A. Spurr and H. Myers, *Quantitative analysis of anatase-rutile mixtures with an x-ray diffactometer*, Anal. Chem. 29 (1957), pp. 760–762.
[39] S. Brunauer, P.H. Emett, and E.J. Teller, *Adsorption of gases in multimolecular layers*, J. Am. Chem. Soc. 60 (1938), pp. 309–319.
[40] G.D. Halsey Jr, *Physical adsorption on nonuniform surfaces*, J. Chem. Phys. 16 (1948), pp. 931–937.

[41] H. Kuhn, S.E. Braslavsky, and R. Schmidt, *Chemical actinometry, IUPAC technical report*, Pure Appl. Chem. 76 (2004), pp. 2105–2146.
[42] C. Wang and J.Y. Ying, *Sol-gel synthesis and hydrothermal processing of anatase and rutile titania nanocrystals*, Chem. Mater. 11 (1999), pp. 3113–3120.
[43] J. Livage, M. Henry, and C. Sanchez, *Sol-gel chemistry of transition metal oxides*, Prog. Solid State Chem. 18 (1988), pp. 259–341.
[44] J. Zhang, M. Yan, F. Chen, and M. Anpo, *Preparation of controllable crystalline titania and study on the photocatalytic properties*, J. Phys. Chem. B 109 (2005), pp. 8673–8678.
[45] Y. Li, T.J. White, and S.H. Lim, *Low-temperature synthesis and microstructural control of titania nano-particles*, J. Solid State Chem. 177 (2004), pp. 1372–1381.
[46] R. Janisch, P. Gopal, and N. Spaldin, *Transition metal-doped TiO_2 and ZnO-present status of the field*, J. Phys.: Condens. Matter. 17 (2005), pp. 657–689.
[47] Q. Zhang, L. Gao, and J. Guo, *Preparation and characterization of nanosized TiO_2 powders from aqueous $TiCl_4$ solution*, Nanostruct. Mater. 11 (1999), pp. 1293–1300.
[48] U. Diebold, *The surface science of titanium dioxide*, Surf. Sci. Rep. 48 (2003), pp. 53–229.
[49] S. Kittaka, K. Matsuno, and S. Takahara, *Transformation of ultrafine titanium dioxide particles from rutile to anatase at negatively charged colloid surfaces*, J. Solid State Chem. 132 (1997), pp. 447–450.
[50] A.R. Khataee, V. Vatanpour, and A.R. Amani, *Decolorization of C.I. acid blue 9 solution by UV/nano-TiO_2, fenton, electro-fenton and electrocoagulation processes: a comparative study*, J. Hazard. Mater. 161 (2009), pp. 1225–1233.
[51] N. Daneshvar, D. Salari, and A.R. Khataee, *Photocatalytic degradation of azo dye acid red 14 in water on ZnO as an alternative catalyst to TiO_2*, J. Photochem. Photobiol. A 162 (2003), pp. 317–3221.
[52] N. Daneshvar, D. Salari, A. Niaie, M.H. Rasoulifard, and A.R. Khataee, *Immobilization of TiO_2 nanopowder on glass beads for the photocatalytic decolorization of an azo dye C.I. direct red 23*, J. Environ. Sci. Health A 40 (2005), pp. 1605–1617.
[53] K. Gray, G. Li, S. Ciston, Z. Saponjic, L. Chen, M. Dimitrijevic, and T. Rajh, *Photooxidation and photoreduction using mixed-phase titanium dioxide*, J. Catal. 253 (2008), pp. 105–110.
[54] R.R. Bacsa and J. Kiwi, *Effect of rutile phase on the photocatalytic properties of nanocrystalline titania during the degradation of p-coumaric acid*, Appl. Catal. B 16 (1998), pp. 19–29.
[55] R.I. Bickley, T. Gonzalez-Carreno, J.S. Lees, L. Palmisano, and R.J.D. Tilley, *A structural investigation of titanium dioxide photocatalysts*, J. Solid State Chem. 92 (1991), pp. 178–190.
[56] V. Grassian, *Environmental Catalysis*, CRC Press, Taylor & Francis Group, USA, 2005.
[57] J.R. Bolton, K.G. Bircger, W. Tumas, and C.A. Tolman, *Figure-of merit for the technical development and application of advanced oxidation technologies for both electric and solar-derived systems*, Pure Appl. Chem. 73 (2001), pp. 627–637.
[58] N. Daneshvar, A. Aleboyeh, and A.R. Khataee, *The evaluation of electrical energy per order (E_{Eo}) for photooxidative decolorization of four textile dye solutions by the kinetic model*, Chemosphere 59 (2005), pp. 761–767.
[59] M.F.J. Dijkstra, H. Buwalda, A.W.F. Jong, A. Michorius, J.G.M. Winkelman, and A.A.C.M. Beenackers, *Experimental comparison of three reactor designs for photocatalytic water purification*, Chem. Eng. Sci. 56 (2001), pp. 547–555.
[60] Y.J. Lin, A. Lee, L.S. Teng, and H.T. Lin, *Effect of experimental factors on nitrobenzaldehyde photoisomerization*, Chemosphere 48 (2002), pp. 1–8.